Lawrence Berkeley National Laboratory
Recent Work

Title
Isomer specific product detection in the reaction of CH with acrolein.

Permalink
https://escholarship.org/uc/item/1t905012

Journal
The journal of physical chemistry. A, 117(43)

ISSN
1089-5639

Authors
Lockyear, Jessica F
Welz, Oliver
Savee, John D
et al.

Publication Date
2013-10-01

DOI
10.1021/jp407428v

Peer reviewed

Isomer Specific Product Detection in the Reaction of CH with Acrolein

Jessica F. Lockyear,[†] Oliver Welz,[‡] John D. Savee,[‡] Fabien Goulay,[§] Adam J. Trevitt,[∥] Craig A. Taatjes,[‡] David L. Osborn,[‡] and Stephen R. Leone*,[†,⊥]

[†]Lawrence Berkeley National Laboratory, 1 Cyclotron Road, Berkeley, California 94720, United States
[‡]Combustion Research Facility, Mail Stop 9055, Sandia National Laboratories, Livermore, California, 94551, United States
[§]Department of Chemistry, West Virginia University, Morgantown, West Virginia, 26506, United States
[∥]School of Chemistry, University of Wollongong, Wollongong, NSW 2522 Australia
[⊥]Departments of Chemistry and Physics, University of California, Berkeley, California 94720, United States

S *Supporting Information*

ABSTRACT: The products formed in the reaction between the methylidene radical (CH) and acrolein (CH_2=CHCHO) are probed at 4 Torr and 298 K employing tunable vacuum-ultraviolet synchrotron light and multiplexed photoionization mass-spectrometry. The data suggest a principal exit channel of H loss from the adduct to yield C_4H_4O, accounting for $(78 \pm 10)\%$ of the products. Examination of the photoionization spectra measured upon reaction of both CH and CD with acrolein reveals that the isomeric composition of the C_4H_4O product is $(60 \pm 12)\%$ 1,3-butadienal and $(17 \pm 10)\%$ furan. The remaining 23% of the possible C_4H_4O products cannot be accurately distinguished without more reliable photoionization spectra of the possible product isomers but most likely involves oxygenated butyne species. In addition, C_2H_2O and C_3H_4 are detected, which account for $(14 \pm 10)\%$ and $(8 +10, -8)\%$ of the products, respectively. The C_2H_2O photoionization spectrum matches that of ketene and the C_3H_4 signal is composed of $(24 \pm 14)\%$ allene and $(76 \pm 22)\%$ propyne, with an upper limit of 8% placed on the cyclopropene contribution. The reactive potential energy surface is also investigated computationally, and specific rate coefficients are calculated with RRKM theory. These calculations predict overall branching fractions for 1,3-butadienal and furan of 27% and 12%, respectively, in agreement with the experimental results. In contrast, the calculations predict a prominent CO + 2-methylvinyl product channel that is at most a minor channel according to the experimental results. Studies with the CD radical strongly suggest that the title reaction proceeds predominantly via cycloaddition of the radical onto the C=O bond of acrolein, with cycloaddition to the C=C bond being the second most probable reactive mechanism.
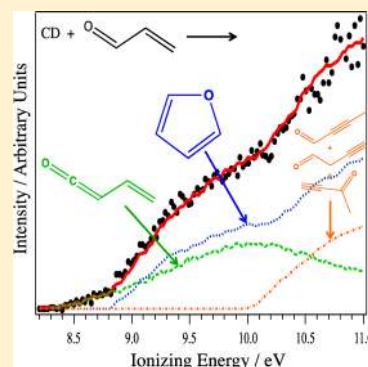
■ INTRODUCTION

Carbonyl compounds are ubiquitous in exhaust gases from combustion engines. One of the carbonyls that is potentially most harmful to human health is acrolein (CH_2=CHCHO), which may account for up to 8% of the aldehydes generated by vehicles[1−4] and has an average tropospheric concentration between 0.5 and 3.186 parts-per-billion.[5] The presence of atmospheric acrolein is primarily attributed to the incomplete combustion of petroleum, biomass, and plastics.[1,4,6,7−9] With the increased use of ethanol−gasoline blends and biodiesel fuels, it has become important to evaluate how the increased oxygen content of such fuels affects the absolute and relative concentrations of aldehydes emitted.[10] Despite the fact that overall hydrocarbon emissions are reduced by introducing an oxygenated functional group to the fuel molecule, it is clear that the relative emissions of the most abundant aldehydes are markedly altered, and generally increased, when combusting oxygenated fuels compared to petroleum-based fuels.[2,4,11−18] The transesterification process used to manufacture biodiesel fuels yields glycerol as a byproduct, which thermally

decomposes to acrolein at relatively low temperatures.[19] Thus, increased acrolein emissions when using biodiesel compared to petro-diesel can be linked to fuel quality and the presence of residual glycerol.[20] In addition, oxidation at 550 °C of rapeseed oil, the precursor to the majority of biodiesel fuels used in Europe, yields high quantities of acrolein and other aldehydes.[21] A more in-depth understanding of combustion engine performance and emissions can be achieved with a detailed knowledge of the primary products, subsequent reactions, and fate of species such as acrolein.[10]

Many radicals and excited state species are involved in the propagation of combustion, one being the highly reactive methylidene (CH) radical.[22−31] CH is, on average, approximately 3 orders of magnitude less abundant than the chain propagator OH in simple methane flames.[24] Nevertheless, the CH radical plays a critical role in the kinetics of NO_x formation

and destruction,[22] evidence that even minor species can strongly influence the formation and destruction of pollutants. The primary formation mechanism for CH in nonpremixed fuel flames is the reaction between CH_2 and OH yielding CH and H_2O.[22] Naik and Laurendeau measured concentrations of CH up to 1−2 ppm in partially mixed and nonpremixed methane-air flames at pressures between 1 and 12 atm.[22] Köhler et al. measured the CH concentration in propene and cyclopentene flames to be around 10−20 ppm.[23] Further studies showed that CH concentrations in flames range from 0.1 to 60 ppm.[25,28,29,30]

Neither the rate coefficient nor products of the reaction between CH and acrolein have been reported in the literature. This manuscript presents isomer-resolved branching results on the products formed by the reactions of CH and CD with acrolein. Reaction rate coefficients of CH with saturated and unsaturated hydrocarbons are reported to be very fast:[32] from 9.74×10^{-11} cm^3 molecule^{-1} s^{-1} with methane[33] to 5×10^{-10} cm^3 molecule^{-1} s^{-1} with toluene[34] at 300 K. A few rate coefficients of CH with oxygenated hydrocarbons have also been determined; those with formaldehyde (CH_2O),[33] methanol (CH_3OH),[35] and ketene (CH_2CO)[36] are measured to be 3.81×10^{-10} cm^3 molecule^{-1} s^{-1} (at 300 K and 20−300 Torr), 2.52×10^{-10} cm^3 molecule^{-1} s^{-1} (at 298 K and 100−600 Torr), and 2.4×10^{-10} cm^3 molecule^{-1} s^{-1} (at 295 K and 5 Torr), respectively. Given the similarity in these rates, it is anticipated that the rate coefficient of CH with acrolein is likely $>1 \times 10^{-10}$ cm^3 molecule^{-1} s^{-1}, close to the gas-kinetic limit. Rate coefficient data coupled with branching fractions into the various product channels, with isomeric specificity, are valuable for the development of accurate combustion models.

Recent experiments in our group measured the products formed upon reaction of CH with acetaldehyde[37] and of CH with propene.[38] Five exit channels were inferred in the CH + acetaldehyde reaction, corresponding to CH_2, HCO, CO, CH_3, and H loss from an initial complex, by detecting either these products or the coproduct(s) of each of these channels. The CH_2-formation channel was attributed to direct H-abstraction by CH, whereas the remaining four exit channels were attributed to either insertion of CH into a C−H bond or cycloaddition to the C=O bond. In the CH + propene reaction the dominant channel was found to be formation of C_4H_6 + H. The C_4H_6 product is composed of three separate isomers: 1,3-butadiene, 1,2-butadiene, and 1-butyne, which can all be attributed to a cycloaddition mechanism of the CH radical to the C=C bond of propene, followed by H-loss.

The CH + acetaldehyde and CH + propene studies highlights an interesting aspect of CH reactivity: the radical exhibits barrierless attack at both C−H sites and unsaturated bonds, by insertion into single bonds and addition or cycloaddition at double bonds, with cycloaddition being the most favorable.[32,39−42] In the case of cycloaddition onto an unsaturated bond, it is well accepted that the mechanism proceeds via cycloaddition across the double bond followed by ring-opening; the cyclic intermediate is extremely short-lived.[34,39,43−45] These addition, insertion, and cycloaddition reactions, which are illustrated in Figure 1 for ethene, often result in molecular weight growth and are therefore of interest in combustion[45] and astrochemical[46,47] environments. Acrolein presents an interesting case study because it contains both C=O and C=C bonds, which in principle allows investigation of the competition between cycloaddition of CH at the C=O and C=C bonds.
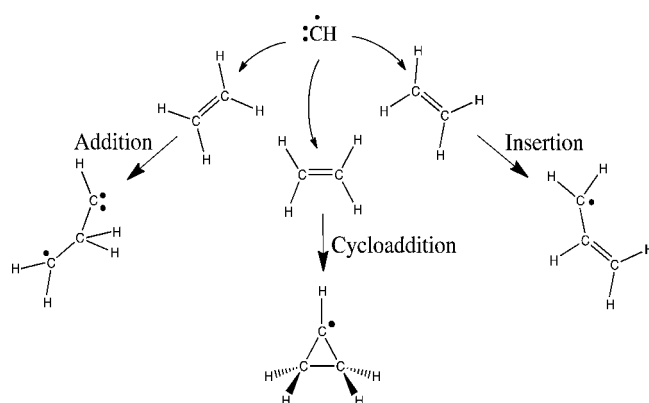

Figure 1. Schematic of addition, cycloaddition, and insertion mechanisms that can occur in the reaction of CH with the unsaturated hydrocarbon ethene.

■ EXPERIMENTAL DETAILS

The chemical reactions take place in a laser photolysis, slow flow reactor, which is coupled to a multiplexed photoionization mass spectrometer at the Advanced Light Source of Lawrence Berkeley National Laboratory. Detailed accounts of the experimental apparatus and method are given elsewhere,[44,48,49] and only a brief overview is presented here. The reactions occur inside a quartz tube at 4 Torr (533 Pa) and 298 K. The gas flow consists of small amounts of the CH radical precursor and acrolein in a large excess of helium buffer gas with around 15% nitrogen. Bromoform ($CHBr_3$ or deuterated bromoform $CDBr_3$) is used as the radical precursor and the laser dissociation of $CHBr_3$ is an effective method to produce CH radicals with high yield.[43,50−53] Liquid bromoform is placed in a glass vessel and kept at a temperature of 8 °C. Helium is bubbled through the liquid at a total pressure of 700 Torr, entraining bromoform in the flow. A 10% gas mixture of acrolein in helium is prepared in a stainless steel cylinder at a total pressure of 2000 Torr. The various components are mixed in situ at the entrance of the reactor using calibrated mass flow controllers. Reactor pressure is maintained with a butterfly valve after the reactor with active feedback control. The total gas flow is 100 sccm (standard cubic centimeters per minute), high enough to completely replenish the gas in the reactor tube between consecutive laser pulses (4 Hz repetition rate).

Gas densities are approximately 1.4×10^{13} cm^{-3} bromoform, 2.6×10^{14} cm^{-3} acrolein, 1.95×10^{16} cm^{-3} N_2, and 1.1×10^{17} cm^{-3} He, at a total gas density of 1.3×10^{17} cm^{-3}. A uniform initial concentration of CH (or CD) radicals is produced in the axial and radial directions of the reactor tube by 248 nm two-photon photolysis of bromoform using an unfocused beam of an excimer laser. The typical photolysis fluence inside the reaction flow tube is around 70 mJ cm^{-2} in a 20 ns pulse. There is effectively no attenuation of the photon flux along the length of the flow tube due to absorption, as verified by the stable concentrations of products of photolytically initiated reactions. The density of nitrogen in the flow is sufficient to quench any vibrationally excited CH/CD radicals formed during the photolysis of bromoform on a time scale faster than the reaction.[39,54] During the photolysis of $CHBr_3$, additional fragments such as $CHBr_2$, CHBr, CBr, HBr, Br, and Br_2 could be formed.[34,50] The radical fragments may all potentially react with acrolein in the flow tube, and the relative significance of these reactions compared to the reaction of interest (CH + acrolein) depends on their concentration and reactivity. The
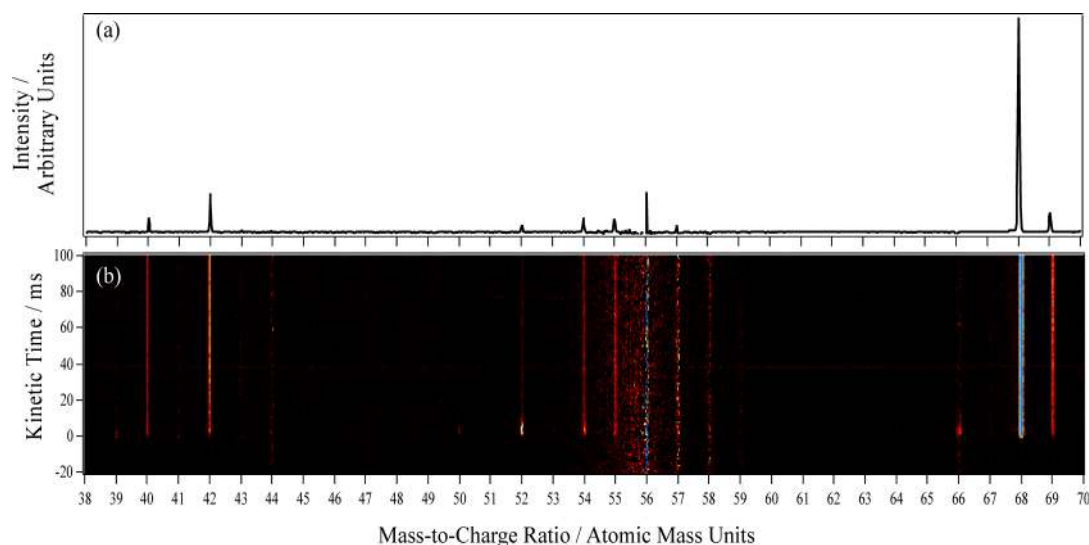
Figure 2. (a) Shows the mass spectrum collected with both $CHBr_3$ and acrolein in the flow reactor at 4 Torr and 298 K, integrated over the 8.2−10.4 eV photon energy range and kinetic times up to 100 ms after photolysis. (b) Shows the mass spectrum in panel a as a function of kinetic time, where the photolysis laser fires at $t = 0$. Data are background corrected by subtraction of the prephotolysis laser signal. The intensity scale goes from black (least counts) via red and yellow to blue (most counts). The main peaks are at m/z = 40, 42, 52, 54, 55, 68, and 69. No signals that could arise from the CH + acrolein reaction are detected at $m/z < 38$. The peak at the parent mass of acrolein (m/z = 56) arises due to saturation of this mass peak, which does not affect signal at other masses.

relative proportion of the fragments formed depends strongly on the photodissociation wavelength. At 248 nm the dominant single-photon process is cleavage of a C−Br bond to give Br + $CHBr_2$.[50] In general, the reactivity of $CHBr_2$ is reported to be at least 2 orders of magnitude lower than that of CH[55,56] and the only products of the $CHBr_2$ + acrolein reaction are likely to be CH_2Br_2 + C_3H_3O. There are three main competing secondary dissociation channels when $CHBr_2$ absorbs a 248 nm photon: CHBr + Br, CH + Br_2, and CBr + HBr.[50] In a transient spectroscopy study at 193 nm, CHBr is formed with a cross-section of 3.42×10^{-18} cm^2 and a yield of 0.3, whereas at 248 nm the CHBr concentration was below the detection limit, suggesting a number density at least 200 times lower than at 193 nm.[50,57] For a 248 nm laser fluence of 70 mJ cm^{-2}, as in the current experiment, this corresponds to a CHBr number density of 6×10^9 cm^{-3}.

The reaction between CH/CD and acrolein occurs uniformly along the axial direction of the reactor as the irradiated gas moves down the tube. A portion of this gas is sampled from the flow tube through a 650 μm diameter pinhole in the side of the tube into a chamber that is typically at a pressure of 10^{-5} Torr. A nearly effusive beam emerges from this pinhole and then passes through a 1.5 mm diameter skimmer before entering a differentially pumped ionization region. The gas beam is crossed by tunable synchrotron undulator vacuum ultraviolet (VUV) radiation that is dispersed by a 3 m monochromator (Chemical Dynamics Beamline at the Advanced Light Source of Lawrence Berkeley National Laboratory). The monochromatic VUV radiation energy is calibrated using known atomic resonances of Xe; at the conditions employed in these experiments the VUV light has a bandwidth of 40 meV. The VUV photon flux at each photon energy is measured using a photodiode (SXUV-100 International Radiation Detectors, Inc.) with a NIST-traceable spectral response calibration. The masses of all cations formed in the ionization region are monitored with an orthogonal acceleration time-of-flight mass spectrometer equipped with a microchannel plate detector.

Mass spectra are taken at intervals of 20 μs, from −20 to 130 ms relative to photolysis. By additionally scanning the photon energy, time- and photon energy-resolved mass spectra are recorded, leading to a three-dimensional data block consisting of ion intensity as a function of m/z (mass-to-charge ratio), reaction time, and photon energy.

The three-dimensional data block can be "sliced" in three ways: m/z vs. kinetic time, m/z vs. photon energy and photon energy vs. kinetic time. Photoionization spectra are constructed by integrating the data first over a time window that corresponds to the production of the species of interest in the photolytically initiated reaction, then over the desired mass-to-charge ratio. Background contributions are removed by subtraction of the average prephotolysis signal taken in the 20 ms before the photodissociation laser pulse. Finally, these background-subtracted signals are normalized for the VUV photon flux at each photon energy. Full time- and photon-energy-dependent spectra are collected three times to check for consistency, with 200 laser pulses at each VUV photon energy. The principal source of noise is "dark counts" at the microchannel plate leading to a very low background signal.

The purities of gases and reactants are as follows: nitrogen, (boil-off from liquid nitrogen); He, 99.999%; bromoform, >99%; D-bromoform 99.5% D atom, with 1% carbon tetrabromide for stabilization; acrolein, >99%.

■ COMPUTATIONAL METHODOLOGY

Identification of the isomers produced in the CH + acrolein reaction relies on fitting the measured product photoionization spectra to known calibration spectra of the pure compounds. In some cases these calibration spectra have not been measured, largely due to the instability of the molecules, and we must simulate the shapes of these spectra in order to determine the best fit to the data. Employing the Gaussian 09 suite of programs,[58] adiabatic ionization energies (AIEs) are calculated using the CBS-APNO composite method.[59] The geometries, harmonic vibrational modes and the transition intensities for

the molecules of interest are calculated at the B3LYP/6-311+
+G(2d,p) level, and photoelectron spectra are simulated
making use of the built-in Franck−Condon overlap feature of
Gaussian 09.[60,61] Integration of the photoelectron spectrum
provides a theoretical photoionization spectrum that we can
compare to the experimental data.[62] Note that this method is
based on the assumption of direct ionization to the lowest-lying
cationic state and does not describe autoionizing and shape
resonances, dissociative ionization, and ionization to excited
cationic states. Where applicable, the semiempirical method of
Bobeldijk et al.[63] is used to estimate the absolute photo-
ionization cross sections. Photoionization spectra used in the
following analysis, simulated or experimental, are given in the
Supporting Information.

Minima and first-order saddle points on the CH + acrolein
potential energy surface (PES) are explored using the CBS-
QB3 method.[64,65] The quantum-chemical calculations are
performed using Gaussian 09.[58] Expectation values of the
total spin squared operator $\langle S^2 \rangle$ and the T1 diagnostics of Lee
et al.[66] are evaluated at unrestricted Hartree−Fock (UHF) and
CCSD(T) levels of theory, respectively, using the 6-31+G(d′)
basis set employed in the CBS-QB3 scheme.[59]

■ RESULTS

Acrolein has a very low absorption cross section of 8.8×10^{-22}
cm^{-2} at 248 nm.[67] With this value, assuming a quantum yield of
unity for photodissociation of acrolein, and typical acrolein
number densities of 2.6×10^{14} cm^{-3}, an upper limit of 4×10^{10}
cm^{-3} is expected for photodissociation products of acrolein.
The principal dissociation channels at 248 nm would yield
CH$_2$CH + HCO and CO + C$_2$H$_4$.[68] Experiments were carried
out without bromoform present in the flow and these potential
photolysis products of acrolein were not detected above the
signal-to-noise limit meaning that photolysis of acrolein does
not significantly contribute to product signal.

The mass spectrum shown in Figure 2a is collected with both
the CH radical precursor (CHBr$_3$) and acrolein in the flow and
integrated over photon energies from 8.2 eV to 10.4 eV and
kinetic times up to 100 ms after photolysis. Because of the
background subtraction, the mass spectrum shows the
difference between the average prephotolysis signal and the
signal from photolysis and subsequent reactions. Positive peaks
in such a spectrum indicate products from direct photolysis,
primary, or secondary chemical reactions. Figure 2b shows the
two-dimensional plot of m/z vs. kinetic time. Time profiles for
each mass peak can be obtained by integrating over the desired
m/z range. For direct closed-shell (whose parent ions appear at
even m/z) products of the CH + acrolein reaction, a temporal
profile is expected that consists of a sharp rise and then a stable
concentration over the time frame of the experiment. For direct
open-shell (appearing at odd m/z) products of the CH +
acrolein reaction the temporal profile should have a sharp rise
and then a decay that reflects the reactivity of the radical
species.

Several peaks are clear in the mass spectrum in Figure 2,
suggesting the possibility of multiple exit channels in the
reaction of CH with acrolein. The principal peak in the
background-subtracted mass spectrum, which can likely be
assigned as a primary product of the CH + acrolein reaction, is
at m/z = 68, loss of H atom from the adduct. There are
additional, minor, peaks at m/z = 40, 42, 52, 54, 55, 66, and 69.
The signal intensity around the mass region of the parent
molecule acrolein peak (m/z = 56) is non-negligible because

the prephotolysis laser background subtraction on such a strong
feature is imperfect. The peaks at m/z = 52 and 66, which have
m/z consistent with closed-shell species, have temporal profiles
that are associated with a radical species (given in Figure S1 in
the Supporting Information). Therefore, these peaks at m/z =
52 and 66 are due to daughter ions from photodissociation of a
heavier radical species and are not considered to arise from a
direct reaction between CH and acrolein. A similar argument is
used to establish that the peaks at m/z = 55 and 69 do not arise
from a direct CH + acrolein reaction; their temporal profiles are
inconsistent with those of radical products (given in Figure S1
in the Supporting Information). The mass-resolution of the
spectrometer is sufficient to distinguish between isobaric
species, those with the same nominal m/z but composed of
different atoms. The precise position of the peak at m/z = 54
reveals that it is due to detection of C$_4$H$_6$, rather than C$_3$H$_2$O.
Because the CH + acrolein reactants combined only have five
H atoms, C$_4$H$_6$ cannot be a direct product of their reaction and
so is also disregarded. These small additional peaks likely result
from primary and secondary reactions of heavier radicals such
as CHBr or CHBr$_2$ with acrolein and other species present in
the flow, followed by dissociative photoionization. The peaks
that have temporal profiles and exact masses commensurate
with direct reaction between CH and acrolein are those at m/z
= 40, 42, and 68. The time traces for the signals at m/z = 40,
42, and 68 are shown in Figure 3.

The most intense peak in Figure 2 is at m/z = 68 and is due
to detection of C$_4$H$_4$O; this would correspond to H-loss from a
complex of CH and acrolein. There are nineteen isomers of
C$_4$H$_4$O; formation of nine of these would require implausible
rearrangements of the constituent atoms of a complex between
the reactants and are not considered. Of the remaining ten
isomers, three are disregarded due to kinetic arguments, details
of which are given in the Supporting Information. Structures
and ionization energies of these twelve isomers that are not
included in the analysis are given in Table S1 in the Supporting
Information with a brief discussion. The seven isomers of
C$_4$H$_4$O that could potentially be formed in the H-loss channel
in the CH + acrolein reaction are shown in Table 1.

In addition to the large peak at m/z = 68, there are two
smaller peaks at m/z = 40 and 42 that are due to detection of
species of the formulas C$_3$H$_4$ and C$_2$H$_2$O, respectively. There
are three possible isomers of C$_3$H$_4$, allene, propyne, and
cyclopropene, and three of C$_2$H$_2$O, ketene, oxirene, and
ethynol. The structures and IEs of these six molecules are
shown in Table 2.

Experiments were carried out to examine the products
formed upon reaction of CD with acrolein. Here isomers
separate by m/z depending on whether they retain the
deuterium atom from CD. Sections of the mass spectra
collected after reaction of the CH and CD radicals with acrolein
are shown in Figure 4. In the CH + acrolein spectrum, there is a
minor peak at m/z = 69 that is larger than the expected 4.4%
[13]C contribution from m/z = 68. Thus, this additional signal at
m/z = 69 is likely to predominantly arise from dissociative
photoionization of a heavier, stable molecule. When using CD
radicals the large peak at m/z = 68 observed in the CH +
acrolein spectrum is still present but reduced in intensity and
the peak at m/z = 69 is larger than in the CH case, implying
contribution to this signal of H-loss channel products. A small
peak appears at m/z = 70 in the CD + acrolein spectrum, which
is due to dissociative photoionization of the same stable
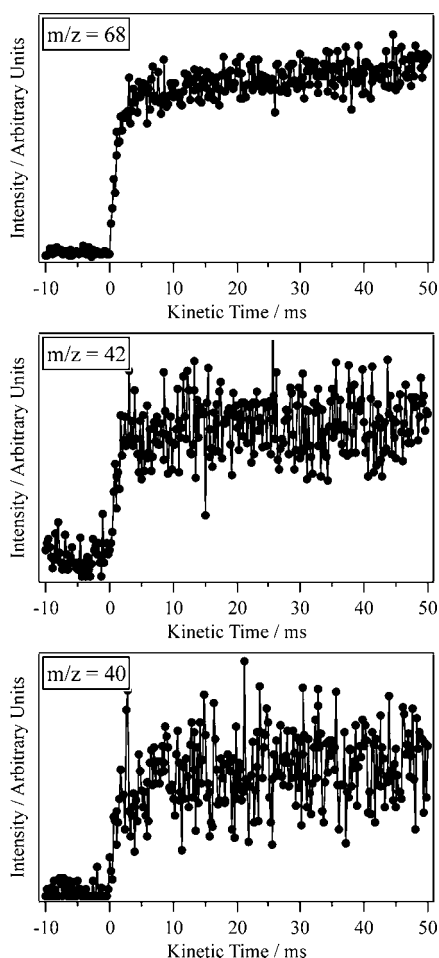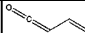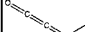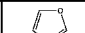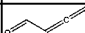molecule responsible for the signal at m/z = 69 in the CH +
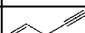
Figure 3. Time profiles for the products at m/z = 68, 42, and 40, integrated over photon energies from 8.2 to 10.4 eV. The photolysis laser is pulsed at t = 0.
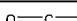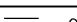
Table 1. Possible Isomers of C_4H_4O Formed in the H-Loss Channel upon Reaction of CH with Acrolein

	Structure	Literature Values for Ionization Energy[a,b] / eV	CBS-APNO Adiabatic Ionization Energy[c] / eV
1,3-Butadienal		8.30–8.45	8.38
1,2-Butadienal		8.68–8.9	8.80
Furan		8.88	8.89
2,3-Butadienal		>9.5[d]	9.95
3-Butynal		9.85–10.2	10.03
3-Butyn-2-one		10.17–10.28	10.18
2-Butynal		10.20–10.28	10.22

[a]Reference 69. [b]Combination of vertical and adiabatic values. [c]This work. [d]Reference 70.

Table 2. Structures and IEs of Isomers of C_3H_4 and C_2H_2O Possibly Formed in the CH + Acrolein Reaction

Molecule	Structure	Literature Values for Ionization Energy[a] / eV	CBS-APNO Adiabatic Ionization Energy[b] / eV
Allene		9.692	9.69
Cyclopropene		9.67	9.73
Propyne		10.36	10.39
Oxirene		N/A	8.60
Ketene		9.617	9.60
Ethynol		N/A	10.01

[a]Reference 69. [b]This work.
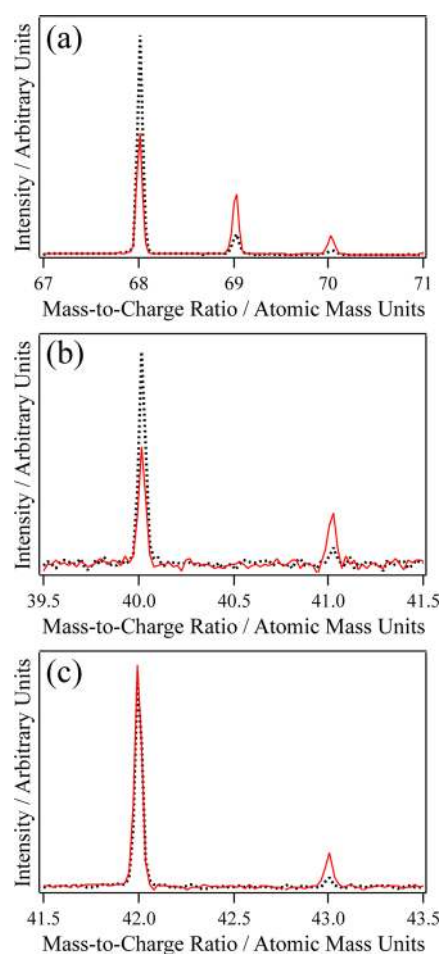
Figure 4. Mass spectra collected following reaction of CH (dotted black line) and CD (solid red line) with acrolein, integrated over photon energies from 8.2 to 10.4 eV. (a) Shows the region from m/z = 67−71, (b) shows the region from m/z = 39.5−41.5, and (c) shows the region from m/z = 41.5−43.5.

acrolein reaction, but in the CD + acrolein case this heavier molecule incorporates the D atom. The peak at m/z = 40 in the CH + acrolein spectrum reduces in relative intensity in the CD + acrolein spectrum and an additional peak appears at m/z = 41. The peak at m/z = 42 in the CH + acrolein spectrum is still present in the CD + acrolein spectrum but there is an additional small peak at m/z = 43.

In order to distinguish the constituent isomers that make up a particular product peak the photoionization spectrum for this signal is compared to known photoionization spectra of possible products. For the H-loss channel (m/z = 68 for CH

+ acrolein and m/z = 68 and 69 for CD + acrolein) the photoionization spectra of the seven possible product isomers shown in Table 1 are needed for the analysis. Of these seven isomers, only the photoionization spectrum of furan has been measured. The photoelectron spectra of 1,3-butadienal,[71] 1,2-butadienal,[71] and 2-butynal[72] have been reported. The integration of a photoelectron spectrum can generally yield an approximation of the shape of the photoionization spectrum.[62] Indeed, the integrated photoelectron spectra of 1,2-butadienal and 2-butynal can be used to approximate the shape of their respective photoionization spectra in the following analysis. However, 1,3-butadienal (also known as vinylketene) contains a ketene-based functional group (O=C=C−). The photoionization spectra of ketene[73] and a variety of substituted ketenes[74] exhibit strong resonances, meaning that the shape of the photoionization spectrum will differ from the integrated photoelectron spectrum. The range of photon energies at which these resonances occur is found to be very similar for ketene, methylketene, ethylketene, and dimethylketene.[74,75] The photoionization spectrum of 1,3-butadienal (vinylketene) might be expected to exhibit such a resonance. Dimethylketene and 1,3-butadienal have the same ionization energy (8.38 eV) and masses different by only 2 amu. Therefore, in the analysis of the m/z = 68 photoionization spectrum, dimethylketene is used as an approximation for that of 1,3-butadienal. For the remaining three isomers (2,3-butadienal, 3-butynal and 3-butyn-2-one), which are not ketene-type species, the photoionization spectra are simulated by integrating their calculated photoelectron spectra, as described above.

The photoionization spectra for the products detected at m/z = 68 for CH + acrolein and m/z = 68 and 69 for CD + acrolein are shown in Figure 5. In each spectrum, the ionization onset is at 8.4 eV, closely matching the literature and calculated values for the IE of 1,3-butadienal, as shown in Table 1. As 1,3-butadienal is the only isomer of C_4H_4O that ionizes at this low energy (the next lowest being 1,2-butadienal at around 8.8 eV and furan at 8.88 eV), the photoionization onset clearly indicates formation of this product in the H- and D-loss channels, even in the absence of an accurate photoionization spectrum for this species. Using dimethylketene as a proxy for 1,3-butadienal introduces a systematic error in the extracted branching ratios, because it is not known how well the dimethylketene spectrum replicates 1,3-butadienal's spectrum. The photoionization spectrum for the signal at m/z = 68 when using CD radicals exhibits a decrease in ionization efficiency at photon energies above 10.5 eV, a feature that is anticipated for ketene-like species due to the expected resonances. This decrease is commensurate with the hypothesis that 1,3-butadienal exhibits a resonant feature and therefore that the photoionization spectrum of dimethylketene is a reasonable substitute for that of 1,3-butadienal.

The photoionization spectrum for m/z = 68 in the CH + acrolein data could potentially include contributions from all seven isomers given in Table 1 and the spectrum itself does not offer many characteristic features to identify these isomers. However, in the CD + acrolein reaction, contributions from D loss can be separated from H loss (Figure 5) at m/z = 68 and 69, revealing structural features of the constituent spectra. The photoionization spectrum at m/z = 68 exhibits a decrease in intensity at photon energies above about 10.5 eV, which is indicative of a ketene-like species. In the m/z = 69 photoionization spectrum the onset at 8.4 eV persists,
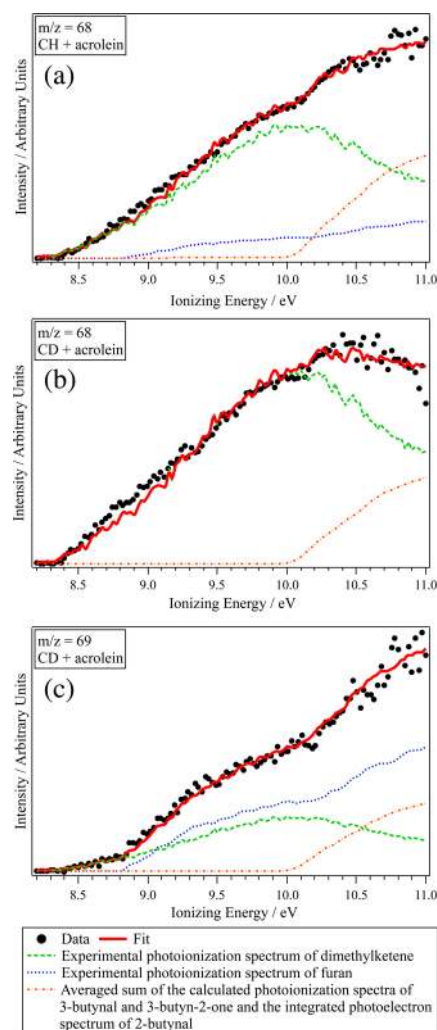

Figure 5. Photoionization spectra for the signals measured at (a) m/z = 68 in the CH + acrolein reaction, (b) m/z = 68 in the CD + acrolein reaction, and (c) m/z = 69 in the CD + acrolein reaction, fitted using the calibration spectra of dimethylketene (green dashed line), furan (blue dotted line), 1,2-butadienal (not shown), 2,3-butadienal (not shown), and a curve that represents the three highest-ionizing isomers: 3-butynal, 2-butynal, and 3-butyn-2-one (orange dot-dashed line). The fit is shown by the solid red line and the constituent species are scaled by their contribution to the fit. It is found that 1,2-butadienal and 2,3-butadienal contribute a fraction of essentially zero to the fit and so their calibration spectra are not shown in the figure.

indicating 1,3-butadienal formation, but there is a sharp increase in intensity around 8.85 eV, indicating another species is formed. To reproduce the shape of the experimental spectrum above 8.85 eV, a contribution from furan must be included. The only other isomer that could account for this increase in the photoionization spectrum at around 8.85 eV (Figure 5) is 1,2-butadienal, but the integrated photoelectron spectrum for this species indicates a more gradual onset at a slightly lower energy. Therefore, the evidence implies formation of furan, a noteworthy finding for combustion chemistry given the important role furan plays in combustion environments, as well as the interesting cyclization step involved. The sum of the dimethylketene and furan spectra does not fully replicate the photoionization spectrum at energies above 10.2 eV. Thus, it is necessary to invoke a further isomer or multiple isomers that

ionize in this photon energy range to explain the observed spectrum.

The close proximity of the IEs and similar shape of the photoionization spectra of 3-butynal, 2-butynal, and 3-butyn-2-one make it difficult to distinguish between these three species to extract a unique fit to the measured spectra for these isomers. Therefore, the calibration spectra of 3-butynal, 2-butynal and 3-butyn-2-one are averaged to give a photoionization spectrum that represents the isomers that ionize at energies between 10.03 and 10.22 eV. Fits were made to the measured photoionization spectra at $m/z = 68$ with CH radicals and $m/z = 68$ and 69 with CD radicals using the calibration curves of five species: dimethylketene, furan, 1,2-butadienal, 2,3-butadienal, and the average of the remaining isomers that ionize at the highest energies; the resultant fits are shown in Figure 5 and the branching ratios are given in Table 3. It is found that

Table 3. Branching Fractions for the Proposed Products of the H-Loss Channel in the CH + Acrolein Reaction (Left-Most Column) and CD + Acrolein Reaction (Two Right-Hand Columns)[a]

Isomer	Branching Fraction / %		
	$m/z = 68$ CH + acrolein	$m/z = 68$ CD + acrolein	$m/z = 69$ CD + acrolein
1,3-butadienal	60 ± 12	$83\ (+17, -22)$	25 ± 10
Furan	17 ± 10	< 14	59 ± 20
1,2-Butadienal	< 10	< 10	< 10
2,3-Butadienal	< 10	< 10	< 10
3-Butynal 2-Butynal 3-Butyn-2-one	23 ± 6	17 ± 6	16 ± 6

[a]Branching fractions are extracted by determining the best fit to the experimental photoionization spectra using a least-squares fitting routine and the calibration spectra of dimethylketene, furan, 1,2-butadienal, 2,3-butadienal, and an average between the 3-butynal, 2-butynal, and 3-butyn-2-one calibration spectra. Errors are given by 2σ. It is found that 1,2-butadienal and 2,3-butadienal have essentially zero contribution to the fit and so an upper limit of 10% is placed on these isomers.

1,2-butadienal and 2,3-butadienal have essentially zero contribution to the fits of the measured photoionization spectra. Hence, an upper limit of 10% is placed on each of the 1,2-butadienal and 2,3-butadienal contributions to the H-loss channel. The remaining three contributions have statistically significant amplitudes, allowing assignment of the product branching fractions, as indicated in Table 3.

To determine the contributions of allene, propyne and/or cyclopropene to the peaks at $m/z = 40$ and 41 in the CH and CD + acrolein data, the photoionization spectra of these species are examined, Figure 6a. Also shown in Figure 6a are the experimentally determined calibration photoionization spectra for allene and propyne[76] and the integrated photoelectron
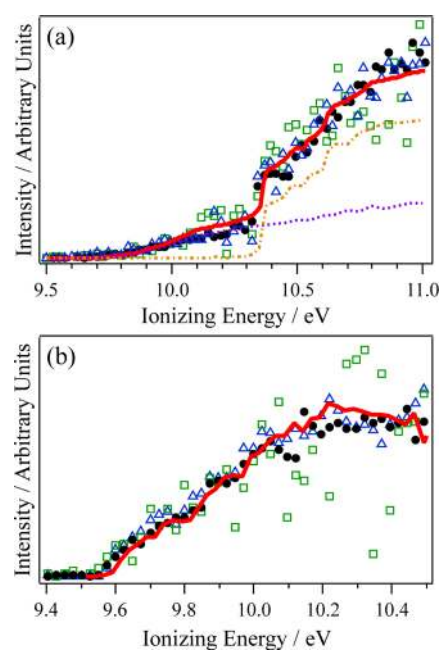

Figure 6. (a) shows the photoionization spectra for $m/z = 40$ in the CH + acrolein data (black circles) and $m/z = 40$ (blue triangles) and 41 (green squares) in the CD + acrolein data. Also shown is the fit (red line) to the black circles, and the experimental photoionization spectra of allene (purple dotted line) and propyne (orange dot-dashed line), with these latter two spectra scaled to show their contribution to the fit. (b) shows the photoionization spectra for $m/z = 42$ in the CH + acrolein data (black circles) and $m/z = 42$ (blue triangles) and 43 (green squares) in the CD + acrolein data, along with the experimental photoionization spectrum of ketene (red line) scaled to the same maximum intensity as the spectrum measured at $m/z = 42$ with CH radicals.

spectrum of cyclopropene, scaled to show their contribution to the fit.[39] Using a least-squares fit to the data collected with CH radicals and the absolute cross sections for the constituent isomers, it is determined that the signal at $m/z = 40$ in the CH + acrolein data and those at $m/z = 40$ (C_3H_4) and $41(C_3H_3D)$ in the CD + acrolein data comprise of $(24 \pm 14)\%$ allene and $(76 \pm 22)\%$ propyne. An upper limit of 8% is placed on the branching fraction of cyclopropene. Errors are given as two standard deviations of the fit parameter for each isomer. The integrated signal at $m/z = 40$ is 2 times larger than that at 41 (shown in Figure 4), indicating a relative C_3H_4: C_3H_3D branching of $(2 \pm 0.2):1$. The peak that was originally at $m/z = 42$ with CH radicals also splits into two peaks upon deuteration of the radical, corresponding to detection of C_2H_2O ($m/z = 42$) and C_2HDO ($m/z = 43$). The photoionization spectra for these signals at $m/z = 42$ in the CH data and $m/z = 42$ and 43 in the CD data, shown in Figure 6b, reveal that ketene[73] is the only isomer of C_2H_2O contributing to these peaks. Oxirene has an IE lower than the experimentally measured ionization onset of the species at $m/z = 42$ and 43 and can therefore be disregarded. The photoionization spectrum of ethynol has been simulated and it is found to have zero contribution to the spectra at $m/z = 42$ and 43. In the CD + acrolein spectrum, the integrated signal at $m/z = 42$ and 43 (shown in Figure 4) give a relative $C_2H_2O:C_2HDO$ branching of $(7 \pm 0.4):1$.

With the estimates of the isomeric composition for each observed peak, in conjunction with the absolute photoionization cross sections of the isomers, it is possible to
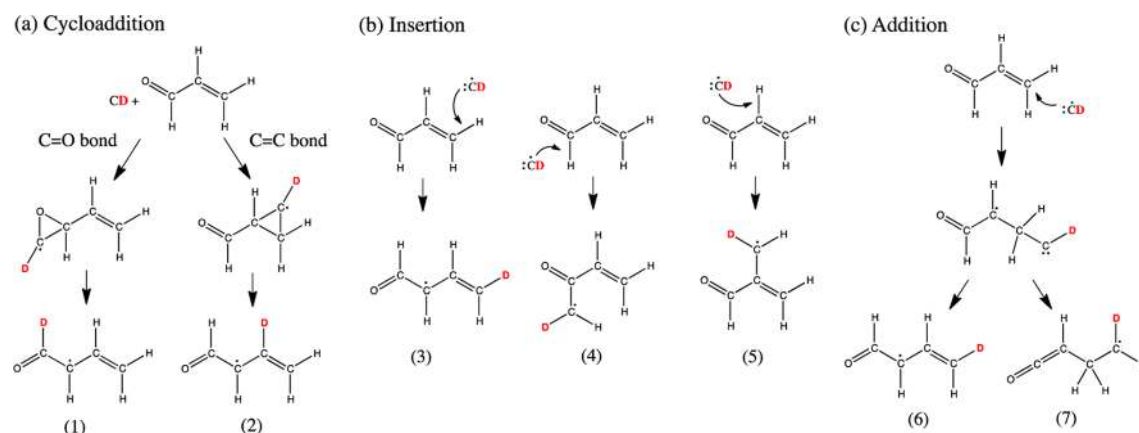
Figure 7. (a) Schematic of the possible CD cycloaddition mechanisms onto either the C=O or C=C bond of acrolein. This mechanism proceeds via a cyclic intermediate that rapidly isomerizes to complexes **1** or **2** after cycloaddition onto C=O or C=C, respectively. The only difference between complexes **1** and **2** is that the D atom that originally resided on the CD radical (in red) attains a different molecular position depending on the cycloaddition site. (b) Schematic of the possible CD insertion mechanisms in the reaction with acrolein. There are three possible sites for CD insertion, which give rise to complexes **3**–**5**. (c) Schematic of the possible addition mechanism in the CD reaction with acrolein, followed by 1,2- or 1,4-H-atom shift giving complex **6** or **7**.

suggest the overall branching into each channel from the peak areas. It is calculated that if the peaks at m/z = 68, 42, and 40 are all indeed due to direct reaction between CH and acrolein, then their relative branching fractions are (78 ± 10)%, (14 ± 10)%, and (8 +10, −8)%, respectively. The error predominantly arises from uncertainties in the shape and absolute magnitude of the photoionization cross-section of the constituent isomers of each peak rather than in the relative areas of the peaks in the mass-spectrum. Therefore a conservative 10% error in the overall relative branching fractions has been estimated.

■ DISCUSSION

Here we discuss the above data in light of potential energy surfaces (PESs) and mechanisms, presenting a partial reactive PES and specific RRKM (Rice−Ramsperger−Kassel−Marcus) theory rate coefficients to rationalize the detected species. In the final section we consider the significance of the findings in the context of combustion chemistry.

There are three initial reaction steps that could take place in the reaction of CH/CD with unsaturated molecules that result in association of the reactants in an encounter complex: addition onto a C site, insertion into a C−H bond, and cycloaddition to the unsaturated site.[34,40,77] Lastly, H-abstraction could occur, which might proceed without intermediate formation of a CH − acrolein complex. After these initial steps, several adducts could be formed, which are shown schematically in Figure 7 and labeled **1**–**7**. To facilitate further mechanistic discussion, the CD radical reaction mechanisms with acrolein are shown in Figure 7 rather than CH. Upon cycloaddition onto C=O (Figure 7a), the radical but-3-enal-2-yl is formed, which is resonant with but-2-enal-4-yl; this radical will be referred to as **1**. Similarly, if cycloaddition is onto C=C then the same resonant structures of but-3-enal-2-yl are formed, referred to as **2**. Insertion of the radical into one of the C−H bonds of acrolein (Figure 7b) would also result in either but-3-enal-2-yl (**3**) or the radical complexes **4** or **5**. Addition of the CH radical onto the terminal carbon site of acrolein (Figure 7c) would result in a carbine radical that could rearrange by 1,2- or 1,4-H-shift to give but-3-enal-2-yl (**6**) or complex **7**, respectively. Although complexes **1**, **2**, **3**, and **6** have

nominally the same but-3-enal-2-yl structure, the D atom from the radical reactant (shown in red) ends up at a different molecular site after cycloaddition, insertion or addition; the position of the D in the encounter complex is dependent on the initial reaction step.

The key result of the experimental investigation is that the photoionization spectra measured at m/z = 68 and 69 in the CD + acrolein reaction are dominated by 1,3-butadienal and furan, respectively. Using the complexes **1**−**7** as starting points, pathways to the formation of furan and 1,3-butadienal are proposed in order to determine the molecular position attained by the D in the furan and 1,3-butadienal products after the CD + acrolein reaction; schematics of these pathways are shown in Figure 8. The complexes labeled **4** and **5**, which arise from insertion of the CH radical into the carbonyl C−H or central C−H bond of acrolein, do not readily rearrange to an intermediate that would undergo H-loss to give furan or 1,3-butadienal. The schematic pathways in Figure 8 suggest that 1,3-butadienal formed via cycloaddition of CD to the C=O bond of acrolein will not incorporate the D atom, thereby appearing at m/z = 68 in the mass spectra, whereas 1,3-butadienal formed via insertion, addition or cycloaddition of CD to the C=C bond of acrolein will incorporate the D, appearing at m/z = 69 in the mass spectra. Furan formed via an initial cycloaddition step would always incorporate the D from the CD radical, thus appearing at m/z = 69 in the mass spectra. Conversely, furan formed *via* the insertion or addition mechanism could eliminate either D or an H from the acrolein and so this product could appear at either m/z = 68 or m/z = 69 in the mass spectra. The observation that, in the CD + acrolein experimental data, the peak at m/z = 68 (D-loss) is dominated by 1,3-butadienal and that at m/z = 69 (H-loss) is dominated by furan, strongly suggests that cycloaddition of the CH to the C=O bond of acrolein is the major initial reaction step. The observation of a small branching fraction of (25 ± 10)% for 1,3-butadienal at m/z = 69 in the CD + acrolein data suggests that cycloaddition to the C=C bond, insertion or addition mechanisms, also play a role in the reactivity, but to a lesser extent. Given that cycloaddition to C=C unsaturated bonds has been observed and has been noted to be more favorable than the insertion or addition mechanisms,[34,37,43] it
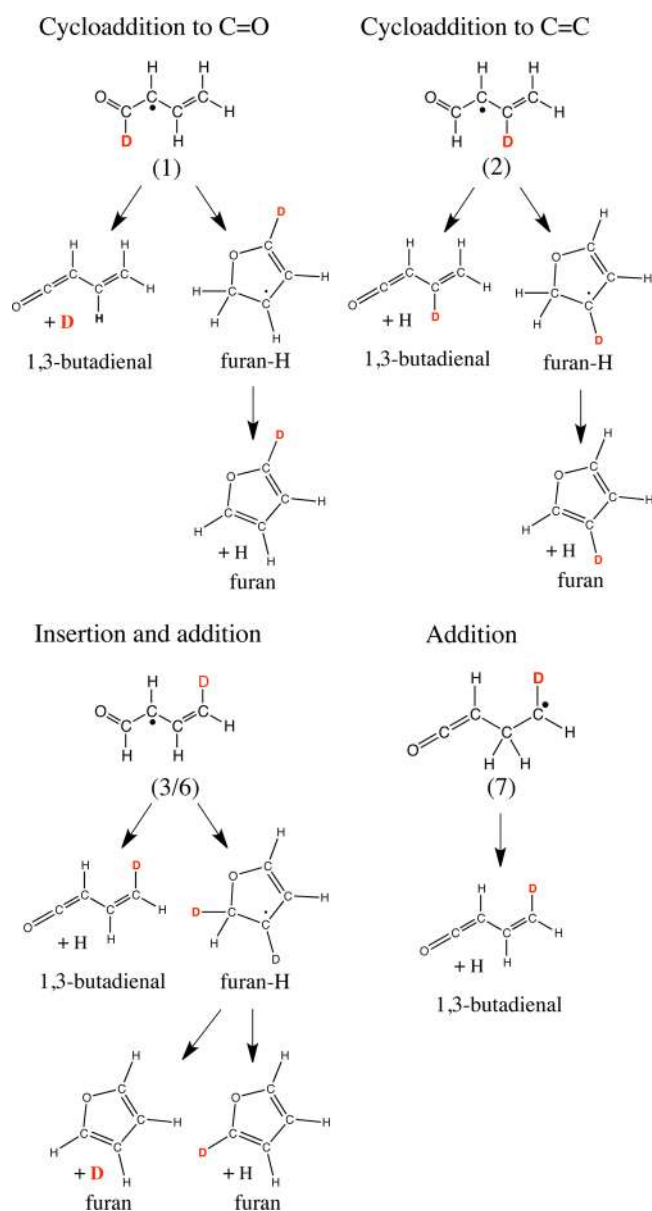
Figure 8. Proposed mechanisms for forming 1,3-butadienal and furan in the CD + acrolein reaction.

seems likely that cycloaddition of the CH radical to the C=C bond of acrolein is the second most probable initial reaction mechanism after cycloaddition to the C=O bond.

In light of the experimental results, a computational investigation of the cycloaddition of CH to both the C=O and C=C bonds of acrolein is carried out. Relevant minima and first-order saddle points on the PES for the CH + acrolein reaction are explored using the CBS-QB3 method and specific rate coefficients calculated employing RRKM theory. These methodologies combined can provide an estimate of the product branching fractions in the CH + acrolein reaction. Pertinent stationary points on the CH + acrolein surface are shown graphically in Figure 9 and a complete list of the species considered can be found in the Supporting Information.

H-loss from the initial C=O and C=C cycloadducts to form 2-ethenyloxirene + H (from the C=O adduct) and 1-cyclopropene-1-carboxaldehyde/2-cyclopropene-1-carboxaldehyde + H (from the C=C cycloadduct) is negligible, as

explained in more detail in the Supporting Information. From the resonantly stabilized but-3-enal-2-yl (referred to as **1−3** and **6** in Figures 7 and 8), cyclization, H-loss, and H-isomerization channels were taken into account. Low-lying decomposition pathways for the cyclization and H-isomerization products were also explored. The calculations predict two energetically low-lying pathways for but-3-enal-2-yl. One of them involves an H-shift via a five-membered ring saddle point to but-2-enal-1-yl. The second pathway involves cyclization to a furan-H adduct, which can subsequently lose an H atom and form furan. As shown in Figure 9, the H-loss channels have substantially higher barriers than product formation involving either cyclization or H-isomerization, but the latter are entropically disfavored over the H-loss channels. Whereas energetic arguments favor the channels with low-lying barriers, entropic effects become increasingly important as the internal excess energy E increases. According to the calculations, formation of but-3-enal-2-yl from CH + acrolein is exothermic by 490 kJ mol^{-1}. Therefore, in the absence of collisional stabilization, and neglecting the thermal distribution in the CH + acrolein reactants, the but-3-enal-2-yl is formed with an internal energy of 490 kJ mol^{-1}, which is substantially above the barriers for isomerization or fragmentation of this radical. To address the question whether the energetically favored, but entropically disfavored channels discussed above, particularly the channel forming furan + H, can compete with the entropically favored H-loss reactions at this high excitation energy, specific rate coefficients $k(E)$ for reactions of but-3-enal-2-yl and its first generation products were calculated using RRKM theory.

All RRKM calculations were carried out employing the rigid rotor/harmonic oscillator approximation. Since essentially all relevant saddle-point structures contain either one or no hindered internal rotations about a C−C (partial) single bond, all internal degrees of freedom were treated as harmonic oscillators. Direct counting procedures for the sums and densities of states were used and $k(E)$ was calculated for a total angular momentum quantum number $J = 0$. For reactions over pronounced saddle points the J-dependence of the specific rate coefficients is usually minor.[78] The results of the RRKM calculations are shown in Figure 10. The competition between energetic and entropic effects on the channel branching can be illustrated by comparing the specific rate coefficients for the cyclization reaction (formation of the furan-H adduct) and 1,3-butadienal + H from but-3-enal-2-yl in Figure 10a. The barrier for cyclization is lower, so that its $k(E)$ curve starts at lower energy. As the internal energy increases, the H-loss channel opens, and the entropic preference of this channel results in the steeper slope of $k(E)$ as a function of internal excess energy compared to $k(E)$ for cyclization. The two $k(E)$ curves cross at $E = 500$ kJ mol^{-1}; at lower energies, cyclization dominates, and at higher energies, 1,3-butadienal + H formation is favored. The vertical line in Figure 10a marks the difference in energy between the CH + acrolein reactants and but-3-enal-2-yl at 0 K, 490 kJ mol^{-1}, which we set equal to the available internal energy of but-3-enal-2-yl. The three dominant reactions of but-3-enal-2-yl at this internal energy, in decreasing order of importance, are 1,4-H shift to but-2-enal-1-yl, cyclization to the furan-H adduct, and H-loss yielding 1,3-butadienal. H-loss yielding 2,3-butadienal is predicted to be a minor channel (see the discussion below), along with H-shift to the oxygen atom and 1,2-H shift to but-3-enal-1-yl. Once formed, the but-2-enal-1-yl and but-3-enal-1-yl radicals preferentially react by α-C−C bond fission to CO + 2-methylvinyl and CO + allyl,
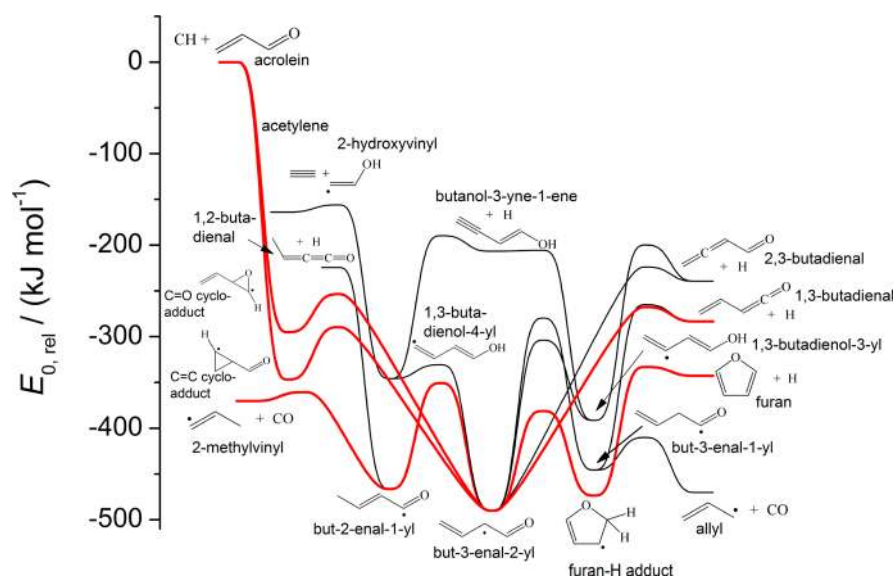
Figure 9. Relevant stationary points on the potential energy surface of the CH + acrolein reaction after addition of CH on the C═C and C═O double bonds in acrolein. Energies are at 0 K (≡, zero-point corrected electronic energies) relative to the CH + acrolein reactants calculated using the CBS-QB3 method. Product channels with branching fractions of >10% as predicted by the RRKM calculations are shown in bold red.
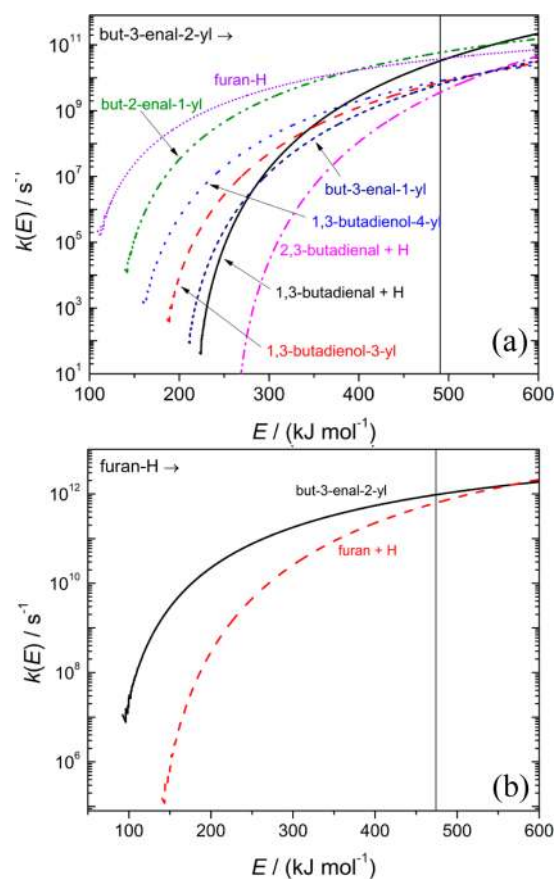

Figure 10. Specific rate coefficients for reactions of (a) but-3-enal-2-yl and (b) the furan-H adduct calculated with RRKM theory. The vertical lines mark the energy of the CH + acrolein reactants relative to but-3-enal-yl and the furan-H adducts, respectively. The calculations use the harmonic frequencies from the B3LYP/6-311G(d,p) level of theory included in the CBS-QB3 scheme, except for the reaction but-3-enal-2-yl → 2,3-butadienal + H, for which frequencies from the M06-2X/6-311++G(d,p) level of theory were employed.

respectively, and back-reaction to but-3-enal-2-yl is unimportant. For the furan-H adduct, however, back-dissociation to but-3-enal-2-yl is predicted to be slightly favored over formation of furan + H, as shown in Figure 10b.

To obtain product branching fractions to bimolecular products in the zero pressure limit at a single energy of but-3-enal-2-yl of 490 kJ mol^{-1}, the set of first-order differential equations was numerically integrated. The resulting branching fractions are shown in Table 4 along with the experimental

Table 4. Predicted Branching Fractions in the CH + Acrolein Reaction, Calculated Using RRKM Theory Based on the Potential Energy Surface Calculated at the CBS-QB3 Level and Harmonic Frequencies at the B3LYP/6-311G(d,p) Level of Theory[a]

Product channel	Theoretical Branching Fraction/%	Total Experimental Branching Fraction/%
2-Methylvinyl + CO	49	<2
1,3-Butadienal + H	27	47 ± 11
2,3-Butadienal + H	3[b]	<8
Furan + H	12	13 ± 8
Allyl + CO	5	<2
Butanol-3-yne-1-ene + H	3	<5

[a]In the right-hand column are the experimental branching fractions for each of the computationally predicted products, which are extracted from the photoionization and mass spectra. [b]The specific rate coefficients for this channel were calculated based on frequencies for the saddle point and but-3-enal-2-yl obtained at the M06-2X/6-311++G(d,p) level of theory.

branching fractions for these products. The remarkable result is that, even at these high internal excitation energies, formation of furan + H involving an entropically disfavored cyclization and the 1,4-H shift *via* a five-membered cyclic transition state can compete with C−H bond-fission reactions that have more entropically favorable transition states. Given the limitations of the current calculations and the errors in branching fractions extracted from experimental photoionization spectra, these

RRKM and experimental results are in fair agreement with regards to the formation of furan and 1,3-butadienal. An accurate estimation of the branching into 2,3-butadienal was hindered by the presence of an unreasonably low vibrational frequency of 12 cm^{-1} for rocking motion of the leaving H atom at the B3LYP/6-311G(d,p) level at the saddle point to 2,3-butadienal + H formation from but-3-enal-2-yl. Such a low frequency has a substantial contribution to the sum of states and would result in a predicted branching fraction for the 2,3-butadienal + H channel of 15%. At the M06-2X/6-311++G(d,p) level of theory[79] this frequency has a more reasonable value of 60 cm^{-1}. For the calculation of the specific rate coefficient for this channel, we therefore used the frequencies for the saddle point and also for the but-3-enal-2-yl reactant obtained at the M06-2X/6-311++G(d,p) level of theory. Using the M06-2X frequencies changed the branching fraction for the 2,3-butadienal + H channel to 3%, a value that is in better agreement with the experimental results. We note that for all other relevant reactions of but-3-enal-2-yl, the specific rate coefficients at 490 kJ mol^{-1} calculated using the harmonic frequencies from the M06-2X calculations agree to within 11% with the rate coefficients derived using the B3LYP frequencies.

The largest discrepancy between the RRKM and experimental branching fractions exists for 2-methylvinyl, where the calculations predict 49% and the experiment suggests <2%. It is conceivable but unlikely that formation of 2-methylvinyl would remain undetected in the present experiments. The 2-methylvinyl can be formed with a maximum internal energy of 370 kJ mol^{-1}, which is much higher than the energy required to decompose this radical; the barrier for fragmentation of 2-methylvinyl into CH_3 + C_2H_2 is 140 kJ mol^{-1} and the barrier for fragmentation into H + propyne is 156 kJ mol^{-1}.[80,81] Substantial decomposition of the hot 2-methylvinyl radicals could explain its absence in the mass spectra. Calculations by Bentz et al. indicate that the CH_3 + C_2H_2 pathway is strongly favored over the H + propyne pathway.[80] Thus, if 2-methylvinyl is formed and then immediately decomposes in our experiments, one might expect methyl radicals (IE = 9.86 eV[82]) to appear in the product mass spectra, but no peak is observed at m/z = 15. The IE of acetylene is 11.4 eV and spectra are measured only up to a photon energy of 11 eV, so the acetylene product would not appear in the data even if it were formed. Although propyne is detected in the experiments, it seems unlikely that it is produced by decomposition of 2-methylvinyl since the CH_3 + C_2H_2 channel is predicted to be more favorable and there is no evidence for methyl radicals in the data.

The observations of allene, propyne, and ketene in the experimental data are also not readily explained by the quantum chemical investigation of the PES for cycloaddition of the CH to the unsaturated bonds of acrolein, and the associated RRKM calculations. The present calculations predict that HCO-loss from but-3-enal-2-yl, or its accessible H-isomerization products, is strongly disfavored compared to CO-loss via α-C−C bond fission. HCO-loss could occur from but-2-enal-3-yl or but-3-enal-3-yl, but the H-isomerization from but-3-enal-2-yl to these isomers involves prohibitively high barriers. The calculations also suggest that there are no favorable low-lying pathways to ketene + C_2H_3 after formation of the but-3-enal-2-yl adduct. The direct coproduct in the ketene formation channel would be the C_2H_3 radical (m/z = 27), which is not observed in the CH + acrolein data. Ketene + C_2H_3 formation from CH + acrolein is exothermic by around 280 kJ mol^{-1}, but H-loss from C_2H_3 to

acetylene + H is endothermic by only 142 kJ mol^{-1} meaning secondary C_2H_3 dissociation is a possibility and may explain the absence of this radical in the mass spectra. Clearly, for a determination of the full branching fractions accounting for collisional stabilization, time-dependent multiple-well master-equation calculations with a more realistic description of anharmonic effects in the internal degrees of freedom and including a treatment of the CH + acrolein cycloaddition, insertion and addition reactions are necessary, which is beyond the scope of the present study. Nevertheless, despite uncertainties, both the computational and experimental investigation suggest comparable branching fractions for 1,3-butadienal and furan formation upon reaction of CH and acrolein.

In the CH + acetaldehyde reaction, an H-abstraction channel was observed, yielding CH_3CO radicals. It was shown that the abstracted hydrogen was exclusively from the more weakly bound aldehydic site of acetaldehyde. An analogous channel in the CH + acrolein reaction would yield the propenoyl radical CH_2CHCO. A small signal is detected at the m/z of propenoyl but it has a time-dependence that indicates that is does not arise from a direct reaction between CH and acrolein. Nevertheless, from the area of this peak it is possible to place an estimate for the maximum branching fraction into the propenoyl-formation channel of 3.5%, suggesting that H-abstraction is not a significant pathway in the CH + acrolein reaction.

◼ CONCLUSIONS AND IMPLICATIONS FOR COMBUSTION

The experimental investigation into the CH + acrolein reaction suggests that three reaction channels take place. These channels correspond to formation of C_4H_4O, C_2H_2O, and C_3H_4 and have branching fractions of (78 ± 10)%, (14 ± 10)%, and (8 +10, −8)%, respectively. Examination of the photoionization spectra measured upon reaction of both CH and CD with acrolein reveals that the isomeric composition of the C_4H_4O product is (60 ± 12)% 1,3-butadienal and (17 ± 10)% furan. Unfortunately, until accurate experimental photoionization spectra are available for all possible isomers it is difficult to decipher which isomers make up the remaining 23% of products in this channel, although the likely candidates that fit the ionization data are oxygenated butyne species. The C_2H_2O that is detected is exclusively ketene and the C_3H_4 signal has a composition of (24 ± 14) % allene and (76 ± 22) % propyne, with an upper limit of 8% cyclopropene.

Studies of the CD + acrolein reaction strongly suggest that the title reaction proceeds predominantly via cycloaddition of the radical onto the C═O bond of acrolein, with cycloaddition to the C═C bond being the second most probable reactive mechanism. Addition to the terminal carbon atom of acrolein and insertion mechanisms probably also play a part in the reactivity and may explain the apparent C_2H_2O and C_3H_4 formation or minor products of the H-loss channel. One might expect cycloaddition mechanisms to both the C═O and C═C bonds of acrolein to be operating in this reaction because these types of mechanism have been shown to take place in the CH + acetaldehyde[37] and CH + propene reactions.[38]

A computational investigation has been undertaken that corroborates the main experimental findings. Specifically, the theoretical branching fractions for the 1,3-butadienal (27%) and furan (12%) products are in fair agreement with those extracted from the experimental data. The remarkable result from both experiment and theory is that the entropically disfavored, but

energetically favored, cyclization reaction leading to furan can compete effectively with H-loss, which is energetically less favored but entropically favored. Such a result is surprising in a system with high internal energy, as is the case in the current investigation of CH + acrolein.

Both experimental and theoretical evidence suggest that one of the major products in the CH + acrolein reaction is furan, an oxygen heterocycle. This is a particularly important product from the combustion chemistry perspective because cyclization and molecular weight growth are involved. Oxygen heterocycles are ubiquitous pollutants emitted from combustion engines.[83] In contrast to the well-known mechanisms of carbon-chain lengthening and cyclization that precede carbocyclic soot formation, the chemistry that leads to higher mass oxygen-containing heterocyclic compounds is not at all well understood. In the context of the current work it is very interesting that comparatively high concentrations of C_xH_yO species have been detected during C_3-oxygenate combustion.[10,84] For example, significant amounts of C_4H_6O, C_4H_8O, and $C_5H_{10}O$ were detected in a propanal flame study.[84] Unfortunately, in this propanal study only the m/z of the species could be determined and not the molecular structures, meaning we can only speculate as to whether these are open-chain (e.g., butanone and butenol) or cyclic (e.g., tetrahydrofuran) isomers.

The reaction of CH with acrolein should be incorporated into combustion models. In particular, understanding this reaction may expand our knowledge of oxygen heterocycle formation during the combustion of oxygenated fuels. More generally, the reactive pathways operating in the CH + acrolein reaction present an interesting competition between entropic and energetic driving forces, which deserve further study.

ASSOCIATED CONTENT

Ⓢ Supporting Information

Temporal profiles of the three principal peaks in the product mass spectrum that likely arise from the reaction between CH and acrolein (Figure S1). The structures and ionization energies of the twelve isomers of C_4H_4O that are not considered as feasible products in the H-loss channel are given (Table S1) with a brief discussion. In addition, the calibration photoionization spectra for each of the individual isomers that have been used to fit the product photoionization spectra are given (Figures S2 and S3). Lastly, the relative energies at 0 K of reactants, intermediates, products and saddle points calculated at the CBS-QB3 level of theory are presented in Table S2. This material is available free of charge via the Internet at http://pubs.acs.org.

AUTHOR INFORMATION

Corresponding Author

*E-mail: srl@berkeley.edu. Phone: (510) 643-5467.

Notes

The authors declare no competing financial interest.

ACKNOWLEDGMENTS

REFERENCES

(1) Bein, K.; Leikauf, G. D. Acrolein - A Pulmonary Hazard. *Mol. Nutr. Food Res.* **2011**, *55*, 1342−1360.

(2) Magnusson, R.; Nilsson, C.; Andersson, B. Emissions of Aldehydes and Ketones from a Two-Stroke Engine Using Ethanol and Ethanol-Blended Gasoline as Fuel. *Environ. Sci. Technol.* **2002**, *36*, 1656−1664.

(3) Zervas, E.; Montagne, X.; Lahaye, J. Emission of Alcohols and Carbonyl Compounds from a Spark Ignition Engine. Influence of Fuel and Air/Fuel Equivalence Ratio. *Environ. Sci. Technol.* **2002**, *36*, 2414−2421.

(4) Song, C. L.; Zhao, Z. A.; Lv, G.; Song, J. N.; Liu, L. D.; Zhao, R. F. Carbonyl Compound Emissions from a Heavy-Duty Diesel Engine Fueled with Diesel Fuel and Ethanol-Diesel Blend. *Chemosphere* **2010**, *79*, 1033−1039.

(5) Faroon, O.; Roney, N.; Taylor, J.; Ashizawa, A.; Lumpkin, M. H.; Plewak, D. J. Acrolein Environmental Levels and Potential for Human Exposure. *Toxicol. Ind. Health* **2008**, *24*, 543−564.

(6) Esterbauer, H.; Schaur, R. J.; Zollner, H. Chemsitry and Biochemistry of 4-Hydroxynonenal, Malonaldehyde and Related Aldehydes. *Free Radic. Biol. Med.* **1991**, *11*, 81−128.

(7) Stevens, J. F.; Maier, C. S. Acrolein: Sources, Metabolism, and Biomolecular Interactions Relevant to Human Health and Disease. *Mol. Nutr. Food Res.* **2008**, *52*, 7−25.

(8) Spada, N.; Fujii, E.; Cahill, T. M. Diurnal Cycles of Acrolein and Other Small Aldehydes in Regions Impacted by Vehicle Emissions. *Environ. Sci. Technol.* **2008**, *42*, 7084−7090.

(9) Woodruff, T. J.; Caldwell, J.; Cogliano, V. J.; Axelrad, D. A. Estimating Cancer Risk from Outdoor Concentrations of Hazardous Air Pollutants in 1990. *Environ. Res.* **2000**, *82*, 194−206.

(10) Kohse-Hoinghaus, K.; Osswald, P.; Cool, T. A.; Kasper, T.; Hansen, N.; Qi, F.; Westbrook, C. K.; Westmoreland, P. R. Biofuel Combustion Chemistry: From Ethanol to Biodiesel. *Angew. Chem.-Int. Ed.* **2010**, *49*, 3572−3597.

(11) Yuan, C. S.; Lin, Y. C.; Tsai, C. H.; Wu, C. C.; Lin, Y. S. Reducing Carbonyl Emissions from a Heavy-Duty Diesel Engine at US Transient Cycle Test by Use of Paraffinic/Biodiesel Blends. *Atmos. Environ.* **2009**, *43*, 6175−6181.

(12) Guarieiro, L. L. N.; de Souza, A. F.; Torres, E. A.; de Andrade, J. B. Emission Profile of 18 Carbonyl Compounds, CO, CO_2, and NO_x Emitted by a Diesel Engine Fuelled with Diesel and Ternary Blends Containing Diesel, Ethanol and Biodiesel or Vegetable Oils. *Atmos. Environ.* **2009**, *43*, 2754−2761.

(13) Lin, Y. C.; Wu, T. Y.; Ou-Yang, W. C.; Chen, C. B. Reducing Emissions of Carbonyl Compounds and Regulated Harmful Matters from a Heavy-Duty Diesel Engine Fueled with Paraffinic/Biodiesel Blends at One Low Load Steady-State Condition. *Atmos. Environ.* **2009**, *43*, 2642−2647.

(14) Tanner, R. L.; Miguel, A. H.; Deandrade, J. B.; Gaffney, J. S.; Streit, G. E. Atmospheric Chemistry of Aldehydes - Enhanced Peroxyacetyl Nitrate Formation from Ethanol-Fueled Vehicular Emissions. *Environ. Sci. Technol.* **1988**, *22*, 1026−1034.

11024

dx.doi.org/10.1021/jp407428v | *J. Phys. Chem. A* 2013, 117, 11013−11026

(15) Grosjean, D.; Grosjean, E.; Gertler, A. W. On-Road Emissions of Carbonyls from Light-Duty and Heavy-Duty Vehicles. *Environ. Sci. Technol.* 2001, 35, 45−53.

(16) Magnusson, R.; Nilsson, C. The Influence of Oxygenated Fuels on Emissions of Aldehydes and Ketones from a Two-Stroke Spark Ignition Engine. *Fuel* 2011, 90, 1145−1154.

(17) Chen, R. H.; Chiang, L. B.; Chen, C. N.; Lin, T. H. Cold-Start Emissions of an SI Engine Using Ethanol-Gasoline Blended Fuel. *Appl. Therm. Eng.* 2011, 31, 1463−1467.

(18) Zhu, R. J.; Cheung, C. S.; Huang, Z. H.; Wang, X. B. Regulated and Unregulated Emissions from a Diesel Engine Fueled with Diesel Fuel Blended with Diethyl Adipate. *Atmos. Environ.* 2011, 45, 2174−2181.

(19) DeWoskin, R. S.; Greenberg, M.; Pepelko, W.; Strickland, J. *Toxicological Review of Acrolein*; U.S. Environmental Protection Agency, CAS No. 107-02-8.

(20) Graboski, M. S.; McCormick, R. L. Combustion of Fat and Vegetable Oil Derived Fuels in Diesel Engines. *Prog. Energy Combust. Sci.* 1998, 24, 125−164.

(21) Pedersen, J. R.; Ingemarsson, A.; Olsson, J. O. Oxidation of Rapeseed Oil, Rapeseed Methyl Ester (RME) and Diesel Fuel Studied with GC/MS. *Chemosphere* 1999, 38, 2467−2474.

(22) Naik, S. V.; Laurendeau, N. M. LIF Measurements and Chemical Kinetic Analysis of Methylidyne Formation in High-Pressure Counter-Flow Partially Premixed and Non-Premixed Flames. *Appl. Phys. B-Lasers Opt.* 2004, 79, 891−905.

(23) Kohler, M.; Brockhinke, A.; Braun-Unkhoff, M.; Kohse-Hoinghaus, K. Quantitative Laser Diagnostic and Modeling Study of C_2 and CH Chemistry in Combustion. *J. Phys. Chem. A* 2010, 114, 4719−4734.

(24) Thoman, J. W.; McIlroy, A. Absolute CH Radical Concentrations in Rich Low-Pressure Methane-Oxygen-Argon Flames via Cavity Ringdown Spectroscopy of the $A^2\Delta$-$X^2\Pi$ Transition. *J. Phys. Chem. A* 2000, 104, 4953−4961.

(25) Mercier, X.; Jamette, P.; Pauwels, J. F.; Desgroux, P. Absolute CH Concentration Measurements by Cavity Ring-Down Spectroscopy in an Atmospheric Diffusion Flame. *Chem. Phys. Lett.* 1999, 305, 334−342.

(26) Heard, D. E.; Jeffries, J. B.; Smith, G. P.; Crosley, D. R. LIF Measurements in Methane Air Flames of Radicals Important in Prompt-NO Formation. *Combust. Flame* 1992, 88, 137−148.

(27) Evertsen, R.; Stolk, R. L.; Ter Meulen, J. J. Investigations of Cavity Ring Down Spectroscopy Applied to the Detection of CH in Atmospheric Flames. *Combust. Sci. Technol.* 1999, 149, 19−34.

(28) Derzy, I.; Lozovsky, V. A.; Cheskis, S. Absolute CH Concentration in Flames Measured by Cavity Ring-Down Spectroscopy. *Chem. Phys. Lett.* 1999, 306, 319−324.

(29) Bonczyk, P. A.; Shirley, J. A. Measurement of CH and CN Concentration in Flames by Laser-Induced Saturation Fluorescence. *Combust. Flame* 1979, 34, 253−264.

(30) Luque, J.; Klein-Douwel, R. J. H.; Jeffries, J. B.; Smith, P.; Crosley, D. R. Quantitative Laser-Induced Fluorescence of CH in Atmospheric Pressure Flames. *Appl. Phys. B-Lasers Opt.* 2002, 75, 779−790.

(31) Smith, G. P.; Luque, J.; Park, C.; Jeffries, J. B.; Crosley, D. R. Low Pressure Flame Determinations of Rate Constants for OH(A) and CH(A) Chemiluminescence. *Combust. Flame* 2002, 131, 59−69.

(32) McKee, K.; Blitz, M. A.; Hughes, K. J.; Pilling, M. J.; Qian, H. B.; Taylor, A.; Seakins, P. W. H Atom Branching Ratios from the Reactions of CH with C_2H_2, C_2H_4, C_2H_6, and neo-C_5H_{12} at Room Temperature and 25 Torr. *J. Phys. Chem. A* 2003, 107, 5710−5716.

(33) Baulch, D. L.; Cobos, C. J.; Cox, R. A.; Esser, C.; Frank, P.; Just, T.; Kerr, J. A.; Pilling, M. J.; Troe, J.; Walker, R. W.; et al. Evaluated Kinetic Data for Combustion Modeling. *J. Phys. Chem. Ref. Data* 1992, 21, 411−734.

(34) Berman, M. R.; Fleming, J. W.; Harvey, A. B.; Lin, M. C. Temperature Dependence of the Reactions of CH radicals with Unsaturated Hydrocarbons. *Chem. Phys.* 1982, 73, 27−33.

(35) Johnson, D. G.; Blitz, M. A.; Seakins, P. W. The Reaction of Methylidene (CH) with Methanol Isotopomers. *Phys. Chem. Chem. Phys.* 2000, 2, 2549−2553.

(36) Hancock, G.; Heal, M. R. Rate-Constant for the Reaction of CH ($X^2\Pi$) with Ketene. *J. Chem. Soc.-Faraday Trans.* 1992, 88, 2121−2123.

(37) Goulay, F.; Trevitt, A. J.; Savee, J. D.; Bouwman, J.; Osborn, D. L.; Taatjes, C. A.; Wilson, K. R.; Leone, S. R. Product Detection of the CH Radical Reaction with Acetaldehyde. *J. Phys. Chem. A* 2012, 116, 6091−6106.

(38) Trevitt, A. J.; Prendergast, M. B.; Goulay, F.; Savee, J. D.; Osborn, D. L.; Taatjes, C. A.; Leone, S. R. Product Branching Fractions of the CH + Propene Reaction from Sychrotron Photoionization Mass Spectrometry. *J. Phys. Chem. A* 2013, 117, 6450−6457.

(39) Goulay, F.; Trevitt, A. J.; Meloni, G.; Selby, T. M.; Osborn, D. L.; Taatjes, C. A.; Vereecken, L.; Leone, S. R. Cyclic Versus Linear Isomers Produced by Reaction of the Methylidyne Radical (CH) with Small Unsaturated Hydrocarbons. *J. Am. Chem. Soc.* 2009, 131, 993−1005.

(40) Nguyen, T. L.; Mebel, A. M.; Lin, S. H.; Kaiser, R. I. Product Branching Ratios of the $C(^3P)$ + $C_2H_3(^2A')$ and $CH(^2\Pi)$ + $C_2H_2(^1\Sigma^+_g)$ Reactions and Photodissociation of H2CC≡CH($^2B_1$) at 193 and 242 nm: An Ab Initio/RRKM Study. *J. Phys. Chem. A* 2001, 105, 11549−11559.

(41) Maksyutenko, P.; Zhang, F. T.; Gu, X. B.; Kaiser, R. I. A Crossed Molecular Beam Study on the Reaction of Methylidyne Radicals $CH(X^2\Pi)$ with Acetylene $C_2H_2(X^1\Sigma^+_g)$ - Competing C_3H_2 + H and C_3H + H_2 Channels. *Phys. Chem. Chem. Phys.* 2011, 13, 240−252.

(42) Zhang, F. T.; Maksyutenko, P.; Kaiser, R. I. Chemical dynamics of the $CH(X^2\Pi)$ + $C_2H_4(X^1A_{1g})$, $CH(X^2\Pi)$ + $C_2D_4(X^1A_{1g})$, and $CD(X^2\Pi)$ + $C_2H_4(X^1A_{1g})$ reactions studied under single collision conditions. *Phys. Chem. Chem. Phys.* 2012, 14, 529−537.

(43) Butler, J. E.; Fleming, J. W.; Goss, L. P.; Lin, M. C. Kinetics of the CH Radical Reactions with Selected Molecules at Room-Temperature. *Chem. Phys.* 1981, 56, 355−365.

(44) Soorkia, S.; Taatjes, C. A.; Osborn, D. L.; Selby, T. M.; Trevitt, A. J.; Wilson, K. R.; Leone, S. R. Direct Detection of Pyridine Formation by the Reaction of CH (CD) with Pyrrole: A Ring Expansion Reaction. *Phys. Chem. Chem. Phys.* 2010, 12, 8750−8758.

(45) Loison, J. C.; Bergeat, A. Rate Constants and the H Atom Branching Ratio of the Reactions of the Methylidyne $CH(X^2\Pi)$ Radical with C_2H_2, C_2H_4, C_3H_4 (Methylacetylene and Allene), C_3H_6 (Propene) and C_4H_8 (Trans-Butene). *Phys. Chem. Chem. Phys.* 2009, 11, 655−664.

(46) Canosa, A.; Sims, I. R.; Travers, D.; Smith, I. W. M.; Rowe, B. R. Reactions of the Methylidine Radical with CH_4, C_2H_2, C_2H_4, C_2H_6, and But-1-ene Studied Between 23 and 295 K with a CRESU Apparatus. *Astron. Astrophys.* 1997, 323, 644−651.

(47) Daugey, N.; Caubet, P.; Retail, B.; Costes, M.; Bergeat, A.; Dorthe, G. Kinetic Measurements on Methylidyne Radical Reactions with Several Hydrocarbons at Low Temperatures. *Phys. Chem. Chem. Phys.* 2005, 7, 2921−2927.

(48) Goulay, F.; Osborn, D. L.; Taatjes, C. A.; Zou, P.; Meloni, G.; Leone, S. R. Direct Detection of Polyynes Formation from the Reaction of Ethynyl Radical (C_2H) with Propyne (CH_3≡CCH) and Allene (CH_2=C=CH_2). *Phys. Chem. Chem. Phys.* 2007, 9, 4291−4300.

(49) Osborn, D. L.; Zou, P.; Johnsen, H.; Hayden, C. C.; Taatjes, C. A.; Knyazev, V. D.; North, S. W.; Peterka, D. S.; Ahmed, M.; Leone, S. R. The Multiplexed Chemical Kinetic Photoionization Mass Spectrometer: A New Approach to Isomer-Resolved Chemical Kinetics. *Rev. Sci. Instrum.* 2008, 79, 104103−104113.

(50) Zou, P.; Shu, J. N.; Sears, T. J.; Hall, G. E.; North, S. W. Photodissociation of Bromoform at 248 nm: Single and Multiphoton Processes. *J. Phys. Chem. A* 2004, 108, 1482−1488.

(51) Fulle, D.; Hippler, H. The High-Pressure Range of the Reaction of CH($^2\Pi$) with N_2. *J. Chem. Phys.* 1996, 105, 5423−5430.

(52) Vaghjiani, G. L. Kinetics of CH Radicals with O_2: Evidence for CO Chemiluminescence in the Gas Phase Reaction. *J. Chem. Phys.* **2003**, *119*, 5388−5396.

(53) Romanzin, C.; Boye-Peronne, S.; Gauyacq, D.; Benilan, Y.; Gazeau, M. C.; Douin, S. CH Radical Production from 248 nm Photolysis or Discharge-Jet Dissociation of $CHBr_3$ Probed by Cavity Ring-Down Absorption Spectroscopy. *J. Chem. Phys.* **2006**, *125*, 114312−114321.

(54) Herbert, L. B.; Sims, I. R.; Smith, I. W. M.; Stewart, D. W. A.; Symonds, A.; Canosa, A.; Rowe, B. R. Rate Constants for the Relaxation of $CH(X^2\Pi,\nu=1)$ by CO and N_2 at Temperatures from 23 to 584 K. *J. Phys. Chem.* **1996**, *100*, 14928−14935.

(55) Rissanen, M. P.; Eskola, A. J.; Timonen, R. S. Kinetics of the Brominated Alkyl Radical ($CHBr_2$, CH_3CHBr) Reactions with NO_2 in the Temperature Range 250−480 K. *Int. J. Chem. Kinet.* **2012**, *44*, 767−777.

(56) Seetula, J. A.; Eskola, A. J. Kinetics of the R+HBr -> RH+Br (CH_3CHBr, $CHBr_2$ or $CDBr_2$) Equilibrium. Thermochernistry of the CH_3CHBr and $CHBr_2$ Radicals. *Chem. Phys.* **2008**, *351*, 141−146.

(57) Chang, B. C.; Guss, J.; Sears, T. J. Hot Bands in the A <- X Spectrum of HCBr. *J. Mol. Spectrosc.* **2003**, *219*, 136−144.

(58) Frisch, M. J.; et al. *Gaussian 09*; Gaussian Inc.: Wallingford, CT, 2009.

(59) Ochterski, J. W.; Petersson, G. A.; Montgomery, J. A., Jr. A Complete Basis Set Model Chemistry. V. Extensions to Six or More Heavy Atoms. *J. Chem. Phys.* **1996**, *104*, 2598−2619.

(60) Santoro, F.; Improta, R.; Lami, A.; Bloino, J.; Barone, V. Effective Method to Compute Franck-Condon Integrals for Optical Spectra of Large Molecules in Solution. *J. Chem. Phys.* **2007**, *126*, 1−13.

(61) Barone, V.; Bloino, J.; Biczysko, M.; Santoro, F. Fully Integrated Approach to Compute Vibrationally Resolved Optical Spectra: From Small Molecules to Macrosystems. *J. Chem. Theory Comput.* **2009**, *5*, 540−554.

(62) Berkowitz, J. Photo-ionization of CH_3OH, CD_3OH and CH_3OD - Dissociative Ionization Mechanisms and Ionic Structures. *J. Chem. Phys.* **1978**, *69*, 3044−3054.

(63) Bobeldijk, M.; Vanderzande, W. J.; Kistemaker, P. G. Simple Models for the Calculation of Photoionization and Electron-Impact Ionization Cross-Sections of Polyatomic Molecules. *Chem. Phys.* **1994**, *179*, 125−130.

(64) Montgomery, J. A.; Frisch, M. J.; Ochterski, J. W.; Petersson, G. A. A Complete Basis Set Model Chemistry. VII. Use of the Minimum Population Localization Method. *J. Chem. Phys.* **2000**, *112*, 6532−6542.

(65) Montgomery, J. A.; Frisch, M. J.; Ochterski, J. W.; Petersson, G. A. A Complete Basis Set Model Chemistry. VI. Use of Density Functional Geometries and Frequencies. *J. Chem. Phys.* **1999**, *110*, 2822−2827.

(66) Lee, T. J.; Taylor, P. R. A Diagnostic for Determining the Quality of Single-Reference Electron Correlation Methods. *Int. J. Quantum Chem.* **1989**, 199−207.

(67) Magneron, I. Unpublished Data; Max-Planck-Institut für Chemie: Mainz, Germany, 1998.

(68) Fang, W. H. A CASSCF Study on Photodissociation of Acrolein in the Gas Phase. *J. Am. Chem. Soc.* **1999**, *121*, 8376−8384.

(69) Linstrom, P. J., Mallard, W. G., Eds.; *NIST Standard Reference Database Number 69*; National Institute of Standards and Technology: Gaithersburg, MD; http://webbook.nist.gov.

(70) Holmes, J. L.; Terlouw, J. K. Structures of $C_4H_4O^+$ Ions Produced from 2-Pyrone and 4-Pyrone. *J. Am. Chem. Soc.* **1979**, *101*, 4973−4975.

(71) Mohmand, S.; Hirabayashi, T.; Bock, H. Gas-Phase Reactions. 22. Thermal Generation of C_4H_4O - Vinylketene and Ethylideneketene. *Chem. Ber.-Recl.* **1981**, *114*, 2609−2621.

(72) Klapstein, D.; Obrien, R. T. The He(I) Photoelectron-Spectra of 2-Butynal and Related Oxyalkynes. *Can. J. Chem.-Rev. Can. Chim.* **1988**, *66*, 143−148.

(73) Yang, B.; Wang, J.; Cool, T. A.; Hansen, N.; Skeen, S.; Osborn, D. L. Absolute Photoionization Cross-Sections of Some Combustion Intermediates. *Int. J. Mass Spectrom.* **2012**, *309*, 118−128.

(74) Goulay, F.; Derakhshan, A.; Maher, E.; Trevitt, A. J.; Savee, J. D.; Scheer, A. M.; Osborn, D. L.; Taatjes, C. A. Formation of Dimethylketene and Methacrolein by Reaction of the CH Radical with Acetone. *Phys. Chem. Chem. Phys.* **2013**, *15*, 4049−4058.

(75) Savee, J. D.; Welz, O.; Taatjes, C. A.; Osborn, D. L. New Mechanistic Insights to the $O(^3P)$ + Propene Reaction from Multiplexed Photoionization Mass Spectrometry. *Phys. Chem. Chem. Phys.* **2012**, *14*, 10410−10423.

(76) Cool, T. A.; McIlroy, A.; Qi, F.; Westmoreland, P. R.; Poisson, L.; Peterka, D. S.; Ahmed, M. Photoionization Mass Spectrometer for Studies of Flame Chemistry with a Synchrotron Light Source. *Rev. Sci. Instrum.* **2005**, *76*, 94102−94109.

(77) Vereecken, L.; Peeters, J. Detailed Microvariational RRKM Master Equation Analysis of the Product Distribution of the C_2H_2 + $CH(X^2\Pi)$ Reaction Over Extended Temperature and Pressure Ranges. *J. Phys. Chem. A* **1999**, *103*, 5523−5533.

(78) Gilbert, R. G.; Smith, S. C. *Theory of Unimolecular and Recombination Reactions*; Blackwell, Oxford, U.K., 1990.

(79) Zhao, Y.; Truhlar, D. G. The M06 Suite of Density Functionals for Main Group Thermochemistry, Thermochemical Kinetics, Non-covalent Interactions, Excited States, and Transition Elements: Two New Functionals and Systematic Testing of Four M06-Class Functionals and 12 Other Functionals. *Theor. Chem. Acc.* **2008**, *120*, 215−241.

(80) Bentz, T.; Giri, B. R.; Hippler, H.; Olzmann, M.; Striebel, F.; Szori, M. Reaction of Hydrogen Atoms with Propyne at High Temperatures: An Experimental and Theoretical Study. *J. Phys. Chem. A* **2007**, *111*, 3812−3818.

(81) Narendrapurapu, B. S.; Simmonett, A. C.; Schaefer, H. F.; Miller, J. A.; Klippenstein, S. J. Combustion Chemistry: Important Features of the C_3H_5 Potential Energy Surface, Including Allyl Radical, Propargyl + H_2, Allene + H, and Eight Transition States. *J. Phys. Chem. A* **2011**, *115*, 14209−14214.

(82) Savee, J. D.; Soorkia, S.; Welz, O.; Selby, T. M.; Taatjes, C. A.; Osborn, D. L. Absolute Photoionization Cross-Section of the Propargyl Radical. *J. Chem. Phys.* **2012**, *136*, 134307−134317.

(83) Durant, J. L.; Busby, W. F.; Lafleur, A. L.; Penman, B. W.; Crespi, C. L. Human Cell Mutagenicity of Oxygenated, Nitrated and Unsubstituted Polycyclic Aromatic Hydrocarbons Associated with Urban Aerosols. *Mutat. Res.-Genet. Toxicol.* **1996**, *371*, 123−157.

(84) Kasper, T.; Struckmeier, U.; Osswald, P.; Kohse-Hoinghaus, K. Structure of a Stoichiometric Propanal Flame at Low Pressure. *Proc. Combust. Inst.* **2009**, *32*, 1285−1292.